PREDICTIONS OF FUEL CHANNEL BEHAVIOUR FOR LARGE LOCA IN CANDU REACTORS

D. J. Oh*, S. Girgis, A. C. D. Wright and R. W. Holmes

AECL CANDU
2251 Speakman Drive
Mississauga, Ontario L5K 1B2

ABSTRACT

This paper describes a model used for fuel channel simulation during large break loss of coolant accidents in CANDU reactors. The model will be used to assess the fuel channel response under conditions in which the pressure tube is heating up and straining.

The model is a detailed idealization of a fuel channel using the CATHENA two fluid code (Reference 1). The model can account for pressure tube temperature non-uniformities due to fuel bearing pad/pressure tube (BP/PT) contact, and for the resulting strain localization.

Simulations of a 20 percent reactor inlet header break in the CANDU 6 design illustrate the capability of the model. Arbitrarily large power pulse was used to check the BP/PT model. Simulations with and without modelling of the heat transfer through a bearing pad to the pressure tube show the effect of bearing pad/pressure tube contact in developing a hot zone on the pressure tube. Finally, a comparison between CATHENA and HOTSPOT (Reference 2) predictions shows good agreement.

^{*} On Attachment From KAERI

INTRODUCTION

1.

This paper describes a model used for fuel channel simulation during large break loss of coolant accidents in CANDU reactors. The model will be used to assess the channel response under conditions in which the pressure tube is heating up and straining.

Following a large break in the heat transport system of a CANDU reactor, fuel channels located nominally downstream of the break void quickly. Fuel cooling is degraded, leading to overheating of fuel and pressure tubes (PT). For certain break sizes and locations, termed critical breaks, this overheating is most severe due to periods of very low flow, and the potential for PT deformation exists. PT deformation depends on the channel coolant pressure during the heatup transient as well as PT temperature and spatial temperature variation. If the channel pressure is high enough, the PT can strain diametrally (ballooning). Because the reactor inlet header (RIH) is the closest of the large diameter piping to the nominally downstream channels, it requires the smallest break size to cause flow stagnation. Thus, the channel pressure remains highest for critical RIH breaks during the high temperature period than for critical breaks in other locations. RIH breaks are limiting for PT ballooning.

Because PT creep strain is a temperature—activated process, PT temperature circumferential non-uniformities result in non-uniform strain. The PT maintains an essentially circular profile as it balloons, but strain and PT thinning is localized.

The model described in this paper is a detailed idealization of a fuel channel using the CATHENA two fluid code (Reference 1). CATHENA is an appropriate tool for this kind of application because, in addition to its two fluid capabilities, the code permits two dimensional (radial and circumferential) conduction modelling of each fuel element (FE) and the PT and incorporates models for thermal radiation, Zr-steam reaction, solid-to-solid contact heat transfer and PT creep, and provides feedback between thermohydraulic and PT strain calculations. A feature of the model is the use of the contact option to model the heat transfer from a FE to the PT via a bearing pad (BP) in contact with the PT. The model can account for PT temperature non-uniformities due to BP/PT contact, and for the resulting strain localization. Whether the hotspots resulting from contact will cause high local strain and possible failure during PT heatup depends mainly on the contact conductance at the BP/PT interface. The contact conductance during LOCA-typical high temperature transients is estimated using data from experiments (Reference 3) performed at AECL Research (WL).

To illustrate the BP/PT model capability, the model is used to simulate the response of a high power channel to a 20 percent reactor inlet header break in the CANDU 6 design. Cases are simulated with and without BP/PT contact modelled to highlight its effect on the PT temperature and strain behaviour. Finally, a comparison between CATHENA and HOTSPOT (Reference 2) predictions is given.

The response of the heat transport system to the 20% reactor inlet header (RIH) break for a CANDU 6 reactor is analyzed using a CATHENA "full-circuit" model. The effects of individual channel characteristics (elevation, feeder geometry, channel power etc.) on fuel and fuel channel behaviour are analyzed by way of "slave" single channel simulations using header boundary conditions predicted by the full-circuit simulations. A node-link model of the fuel channel assembly is constructed and the transient thermohydraulic header boundary conditions from the full-circuit simulations (pressure, enthalpy and void fraction) are applied to the inlet and outlet header. In this way, the fuel channel becomes a "slave" to the applied boundary conditions since the thermohydraulic response of the fuel channel does not feed back to the headers. The following sections summarize the features of each model.

2.1 MODELLING ASSUMPTIONS

2.1.1 Slave Channel Model

The CATHENA model used to assess the channel response to a large LOCA is illustrated in Figures 1 and 2. Figure 1 shows the nodalization of channel S11. Channel S11 is selected because of its peaked flux shape in the nominal core configuration. The fuel channel is divided axially into 12 nodes corresponding to the 12 fuel bundles.

Figure 2 illustrates the CATHENA model for fuel and fuel channel using a 37-element fuel bundle cross section. Since there is a symmetry about the vertical axis of a fuel channel cross section, only a half channel is shown in Figure 2. The model provides a detailed idealization of the fuel, pressure tube and calandria tube. The main features and assumptions of the model are summarized as follows:

- a. The channel power of channel S11 is normalized to the maximum operating limit of 7.3 MW. Table 1 gives the channel axial power distribution. Channels with lower channel power would have increased margin to PT failure.
- b. The BP/PT contact is modelled to occur at the top of the channel at bundle 6. Although contact would only occur near the bottom, it is conservative to assume that it occurs at the hottest location on the PT.
- c. Two-dimensional (radial and circumferential) heat conduction is modelled for each fuel element, for the PT and for the calandria tube (CT). Each fuel element is divided into 4 radial regions: UO₂, gap, Zircaloy sheath and ZrO₂ layer on the outside surface of the sheath. The ZrO₂ layer is included to model the Zr-steam reaction. These fuel element regions are represented by 6, 2, 2 and 2 radial nodes respectively. Each fuel element (except the centre and top element) is circumferentially divided into two sectors primarily to capture the different "inside" and "outside" surface temperatures for the thermal radiation calculation. The centre element has one sector while the top element has eighteen sectors. Adequate circumferential subdivision of the top element is chosen to accurately model the thermal and mechanical response in the vicinty of the BP/PT contact. Both the PT and the CT are divided into 32 circumferential sectors (i.e. 16 in the half channel model shown in Figure 2).

- d. For each sector on each fuel element and the PT, the code calculates whether the sector is in contact with steam, liquid or two-phase fluid, and applies the appropriate convective heat transfer as given in Reference 1.
- e. Thermal radiation is modelled among the fuel elements, between the fuel elements and the PT and between the PT and the CT. The geometry of the channel is assumed concentric. A constant emissivity of 0.8 (based on ZrO₂) is used for the fuel sheaths and the inside surface of the PT and an emissivity of 0.325 (based on unoxidized Zr) is used for the CT and the outside surface of the PT.
- f. Heat generation from Zr-steam reaction both on the sheath outside surface and the inside surface of PT is modelled. The Urbanic-Heidrick correlation (Reference 4) is used for this analysis. The thickness of the oxide layer, volume of hydrogen produced, and the heat generated for the metal surfaces is calculated. The effect of the generated hydrogen in reducing the amount of steam available for the reaction is modelled. This "steam starvation" calculation does not feed back to the channel thermohydraulic calculation.
- g. The fuel-to sheath gap conductance of 10 kW/m².°C is assumed. The conductance value is based on Ross and Stoute's experimental measurements (Reference 5).
- h. PT deformation is modelled for each sector on the PT. CATHENA tracks PT thinning in each circumferential sector, and predicts failure based on Shewfelt's upper and lower bound failure criteria (Reference 6). The default scratch depth of 0.013 mm is assumed to occur at the hottest node of the PT. Pre-test measurements of pressure tube specimens indicated that variations in wall thickness are less than 0.013 mm (Reference 6).
- i. MATPRO Version 11 (Reference 7) fuel properties are used. These are the standard properties used by CATHENA.
- j. Default CATHENA heat transfer and CHF correlations are used. In particular, the Groeneveld table (Reference 8) is used for CHF prediction and the default Berenson correlation (Reference 9) for the post-dryout correlation. The Berenson correlation is a pool-boiling correlation which is expected to underpredict heat transfer at higher flows.
- k. A solid-solid contact model available in CATHENA is used to model the BP/PT contact. There is no explicit bearing pad model in CATHENA, so the contact between a fuel element and the pressure tube (PT) at a bearing pad (BP) location is modelled as a fuel element/pressure tube contact with an effective contact conductance. The effective fuel element to pressure tube contact conductance is calculated by taking into consideration the effects of conduction through the BP, heat transfer to the coolant, and the contact conductance between the BP and the PT. The method used to calculate the effective fuel element to pressure tube heat transfer coefficient is given in Section 2.1.1.1. A standard bearing pad geometry for CANDU 6 fuel bundle is modelled as shown in Figure 3. Since there is no axial conduction in the model, the contact is effectively modelled as occurring

over the full length of the bundle, which is chosen to be the highest power bundle in the fuel channel – bundle 6.

2.1.1.1 Estimate of Effective Heat Transfer Coefficient

This section describes a calculation method to estimate the effective heat transfer coefficient between the fuel element and the pressure tube through the bearing pad. It takes into account the effects of conduction through the bearing pad, heat transfer to the coolant, and the contact conductance between the BP and the PT.

Figure 4 illustrates the model. It is assumed that the sheath temperature, T_s , the coolant temperature T_{ST} , the pressure tube temperature T_{PT} , and the bearing pad-to-coolant heat transfer coefficient h_{ST} are known from the previous time step. The model then solves for the average bearing pad temperature T_{BP} , which in turn, provides the heat transfer to the pressure tube. Knowing the heat transfer and the temperature difference between the sheath and the pressure tube then defines the effective heat transfer coefficient.

In steady state:

$$Q_1 = \frac{K}{L_1} A_1 (T_S - T_{BP})$$
 (1)

$$Q_2 = \left(\frac{1}{K/L_2} + \frac{1}{h_{ST}}\right)^{-1} A_2 (T_{BP} - T_{ST})$$
 (2)

$$Q_3 = Q_1 - Q_2 = \left(\frac{1}{K/L_1} + \frac{1}{h_C}\right)^{-1} A_3 (T_{BP} - T_{PT})$$
 (3)

where:

 Q_1 = power from fuel element (FE) to BP

 Q_2 = power from BP to coolant

 Q_3 = power from BP to PT

 A_1 = contact area between FE and BP

 $A_2 = BP$ surface area in contact with coolant

 A_3 = contact area between BP and PT

 $L_1 = \frac{1}{2}$ of BP height as shown in Figure 4

 L_2 = average distance of BP "centre" to surface

 T_S = sheath temperature

 T_{BP} = average BP temperature

 T_{ST} = coolant temperature

 $T_{PT} = PT$ temperature

K = thermal conductivity of Zr-4

h_{ST} = BP-to-coolant heat transfer coefficient

h_c = BP-to-PT contact conductance

solving for T_{BP}:

$$T_{BP} = \left[\left(\frac{1}{K/L_1} + \frac{1}{h_C} \right)^{-1} A_3 T_{PT} + \left(\frac{1}{K/L_2} + \frac{1}{h_{ST}} \right)^{-1} A_2 T_{ST} + \frac{K}{L_1} A_1 T_S \right]$$

$$X \left[\left(\frac{1}{K/L_1} + \frac{1}{h_C} \right)^{-1} A_3 + \left(\frac{1}{K/L_2} + \frac{1}{h_{ST}} \right)^{-1} A_2 + \frac{K}{L_1} A_1 \right]^{-1}$$
(4)

An effective heat transfer coefficient (\overline{h}) is defined as follows:

$$Q_1 - Q_2 = \overline{h}A_3 (T_S - T_{PT})$$

i.e.,
$$\overline{h} = \frac{Q_1 - Q_2}{A_3(T_S - T_{PT})}$$
 (5)

 T_{BP} is calculated from (4), and by substituting in (3), Q_1 - Q_2 is calculated. By substituting in (5), \overline{h} is evaluated.

2.1.2 The BP/PT Contact Conductance

The BP/PT contact conductance represents the largest uncertainty in this analysis. A recent analysis of transient BP/PT contact experiments with the ANSYS code (Reference 3) suggests a contact conductance with a 3-step form as a function of temperature. It is not completely clear how to translate the 3-step contact conductance of Ar/O_2 gas to that of D_2O , but Reference 3 states that it should be approximately 3 kW/m².°C in the range 600 °C to 1000 °C. For the analysis, the bearing pad to pressure tube contact conductance is assumed to be 1 kW/m².°C when the PT-top element interface temperature is less than 600 °C and 3 kW/m².°C when the PT-top element interface temperature is equal to or greater than 600 °C. The PT-top element interface temperature is defined to be $(T_S + T_{PT}) / 2$ where T_S and T_{PT} is defined in Section 2.1.1.1.

ANALYSIS RESULTS

3.

The initial temperatures for all solid components were obtained from a steady state simulation under initial inlet and outlet header conditions as given in Table 2. Transient thermohydraulic boundary conditions were obtained from a test run of CATHENA full-circuit analysis for the 20% RIH break. The power pulse was arbitraily amplified to test the capability of the model to predict PT failure. The assumed overpower transient used in the analysis is shown in Figure 5. Two cases are considered: one case without BP/PT contact and the other case with the BP/PT model described in Section 2. A comparison between CATHENA and HOTSPOT predictions is performed for the case without BP/PT contact. BP/PT contact cannot be modelled in the current HOTSPOT version.

3.1 CASE 1: BP/PT NOT MODELLED

This is a 20% RIH break case without BP/PT contact. No PT failure based on Shewfelt's upper and lower bound failure criteria was predicted, but PT/CT contact for bundle 6 occurred at 50 s. The minimum local pressure tube thickness at the time of contact is 75% of the original PT thickness.

The fuel channel coolant pressure, void fraction and flow transients at axial node 6 are shown in Figures 6–8 respectively. Initial rapid flow drop due to break occurs in 4 s. Then, up to approximately 38 s, the flow remains low and positive as it is affected by competing forces of the break and PHT pumps. Beyond 38 s, the PHT pumps have voided sufficiently that the channel flow begins to be dominated by the break force. The channel flow stagnates again around 38 s and then reverses at 43 s.

Figure 9 shows the top element top sector (Sector 48 in Figure 2) sheath temperature. The maximum temperature of 1200 °C is reached at 4 s. The sharp sheath temperature rise during the early transient is due to early sheath dryout following the aforementioned initial rapid flow drop.

Figure 10 shows the temperature at the inside surface of the PT top sector (Sector 64 in Figure 2). The PT contacts its CT at 50 s with a contact temperature and pressure of 790 °C and 4.3 MPa respectively and cools down. The circumferential temperature distribution at 46.8 s (the PT failure time in Section 3.2) is shown in Figure 11. The nearly flat temperature distribution for upper half part of PT is characteristic of a steam–exposed PT in a fully voided channel.

The rate of temperature increase of about 100 °C/s between 20 s and 50 s is nearly linear due to the relatively uniform PT heating during this period. The convective and radiative heat flux transients shown in Figure 12 demonstrate relatively uniform PT heatup between 20 s and 50 s.

3.2

To assess the effect of BP/PT contact on the PT temperature predictions, a simulation is performed with the BP/PT model using a contact conductance of 1 kW/m².°C below the interface temperature of 600 °C and 3 kW/m².°C above the interface temperature of 600 °C. PT failure was predicted at 46.8 s based on Shewfelt's lower bound failure criterion. The PT failure occurs at the hottest sector (Sector 64 in Figure 2), i.e., BP/PT contact sector. The failure occurs prior to PT/CT contact. The minimum local pressure tube thickness at the time of failure is 42% of the original PT thickness.

The effect of the BP/PT contact model on the temperature transients of the top element and PT top sectors is shown in Figures 9 and 10 respectively. The temperature of the PT top sector is increased by 65 °C and the top element top sector sheath temperature is decreased by 97 °C at 46.8 s (the PT failure time) due to the effect of BP/PT contact.

The circumferential PT temperature distribution is given in Figure 11 which shows the effect of the contact model in creating a hotspot (65 °C) on the pressure tube at 46.8 s. The BP/PT contact causes the top sector of PT to increase in temperature by 65 °C and the effect is local.

3.3 COMPARISON WITH HOTSPOT SIMULATION

A simulation using HOTSPOT is performed to compare with a CATHENA/SLAVE simulation for the 20% reactor inlet header break. CASE 1 is chosen for comparison because BP/PT contact cannot be modelled in HOTSPOT. The HOTSPOT input values are chosen to be consistent with the CATHENA/SLAVE run conditions.

Coolant temperature is one of the thermohydraulic parameters obtained from the CATHENA/SLAVE simulation to be used for HOTSPOT. However, two coolant temperatures are available from CATHENA; liquid and vapour temperatures, because CATHENA is a two-fluid code. HOTSPOT requires only one coolant temperature. For the present run, the vapour temperature was chosen as coolant temperature for film boiling and single-phase steam convective cases at a heat transfer surface and a mixing temperature (T_{mix}) was chosen otherwise. T_{mix} is obtained from the following equation:

$$T_{\text{mix}} = T_f + \alpha \left(T_g - T_f \right) \tag{6}$$

Where,

 T_f = liquid temperature, T_g = vapour temperature, and α = void coefficient. Circumferential node sectoring in the HOTSPOT simulation is shown in Figure 13. From Figures 2 and 13, it can be seen that Sector 2 in Figure 13 for HOTSPOT corresponds to Sector 48 in Figure 2 for CATHENA. HOTSPOT has only one sector for the PT whereas CATHENA has 32 sectors for the PT. For the present test case, Sector 64 in Figure 2 was chosen as a corresponding sector for Sector 1 in Figure 13 for PT comparison. HOTSPOT assumes uniform deformation of the single–sectored PT in the circumferential direction while CATHENA calculates local deformation of each sector for the 32–sectored PT.

Figures 14 and 15 show the temperature transients of the PT inside surface (Sector 1 in Figure 13 and Sector 64 in Figure 2) and top element outside surface (Sector 2 in Figure 13 and Sector 48 in Figure 2) respectively. Comparison of the PT inside surface temperature predictions of HOTSPOT and CATHENA shows good agreement for times less than 49 s. Temperatures from the two codes differ by less than 5 °C. Predicted contact times are 49 s and 50 s from HOTSPOT and CATHENA respectively. The earlier contact in HOTSPOT calculation is due to the fact that the thermohydraulic boundary conditions of the hottest sector (Sector 48 in Figure 2) in CATHENA are used for HOTSPOT calculation of the single–sectored PT (Sector 1 in Figure 13), leading to the higher average PT temperature and therefore larger average PT deformation in HOTSPOT than in the CATHENA simulations. The differences in temperatures after contact are mainly attributed to the different contact times, and the different moderator models in the two codes.

Comparison of the sheath outside surface temperature prediction of HOTSPOT and CATHENA gives good agreement as shown in Figure 15. Temperature differences between the two codes are less than 25 °C. The differences are attributed to the different thermal radiation environments resulting from the different sectoring schemes in the two codes as shown in Figures 2 and 13.

4. CONCLUSIONS

A model for fuel channel analysis of large break loss of coolant accidents using the CATHENA two fluid code is described.

Simulations of a 20 percent reactor inlet header break in the CANDU 6 design illustrate the capability of the model. Arbitrarily large power pulse was used to check the BP/PT model. Simulations with and without modelling of the heat transfer through a bearing pad to the pressure tube show the effect of bearing pad/pressure tube contact in developing a hot zone on the pressure tube.

The CATHENA simulation without bearing pad modelling is compared with a HOTSPOT code simulation of the same event. The CATHENA results are in good agreement with HOTSPOT.

5. ACKNOWLEDGEMENT

The authors would like to thank Mr. D. McAllister (AECL-CANDU) and Mr. J. Mallory (AECL-WL) for helping set up View Factor Matrices, and Mr. N. K. Popov (AECL-WL) for helping obtain convective heat transfer coefficients from CATHENA to be used for HOTSPOT.

6.

REFERENCES

- 1. D.J. Richards, "Validation of CATHENA Two-Fluid Code", Third International Topical Meeting on Reactor Thermal Hydraulics and Operations, Seoul, Korea, November 14–17, 1988.
- 2. A.P. Muzumdar, R.L. Sakaguchi and J.K. Presley, "HOTSPOT-II: Fuel Bundle Thermal Response Code", Ontario Hydro Nuclear Studies and Safety Department, Report No. 83058, 1983 April.
- 3. A.P. Muzumdar, G.R. Berzins, M. Krause and J.W. DeVaal, "ANSYS Thermal Analysis of Bearing Pad/Pressure Tube Interface", presented at the Third International Conference on Simulation Methods in Nuclear Engineering, 1990 April 18, Montreal.
- 4. V.F. Urbanic and T.R. Heidrick, "High Temperature Oxidation of Zircaloy-2 and Zircaloy-4 in Steam", AECL-6149, 1978.
- 5. A.M. Ross and R.L. Stoute, "Heat Transfer Coefficient Between UO₂ and Zircaloy-2", AECL-1552, 1962.
- 6. R.S.W. Shewfelt and D.P. Godin, "Verification Tests for GRAD, a Computer Program to Predict the Nonuniform Deformation and Failure of Zr-2.5 wt% Nb Pressure Tubes During a Postulated Loss-of-Coolant Accident", AECL-8384, 1985 March.
- 7. "MATPRO-Version 11 (Revision 1) A Handbook of Material Properties for Use in the Analysis of Light Water Reactor Fuel Rod Behavior", NUREG/CR-0497, TREE-1280, Rev 1, February 1980.
- 8. D.C. Groeneveld, S.C. Cheng and T. Doan, "1986 AECL—UO Critical Heat Flux Lookup Table", Heat Transfer Engineering, Vol. 7, pp. 46–62, 1986.
- 9. P.J. Berenson, "Film Boiling Heat Transfer from a Horizontal Surface", Journal of Heat Transfer, Vol. 83, pp. 351–358, 1961.

TABLE 1
CHANNEL AXIAL POWER DISTRIBUTION

Node (Bundle)	Normalized Power (kW) *			
1	177			
2	430			
3	602			
4	694			
5	864			
6	928			
7	923			
8	861			
9	683			
10	572			
11	400			
12	166			
Total	7300			

^{*} The channel power of Channel S11 is normalized to the operating limit of 7.3 MW.

TABLE 2
STEADY STATE HEADER BOUNDARY CONDITIONS

	Inlet Header	Outlet Header 9.987		
Pressure (MPa)	11.345			
Vapour Enthalpy (MJ/kg)	2.505	2.529		
Liquid Enthalpy (MJ/kg)	1.123	1.351		
Void Fraction	0.0	0.281		

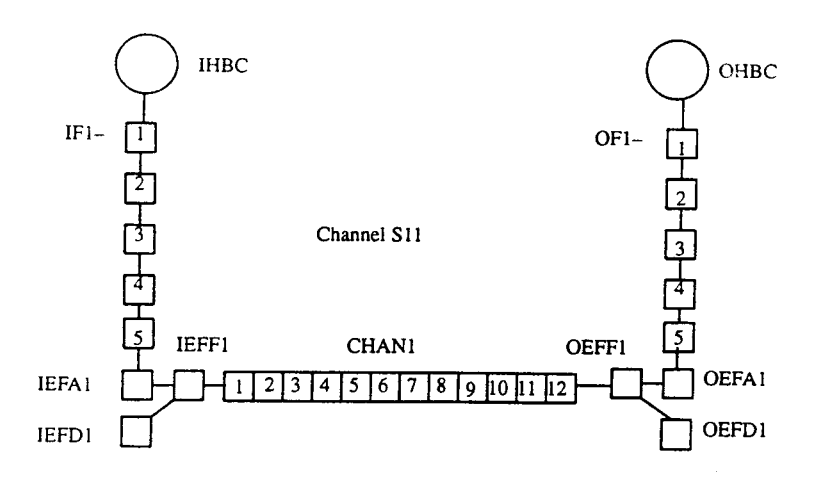


FIGURE 1 Slave Channel Nodalization

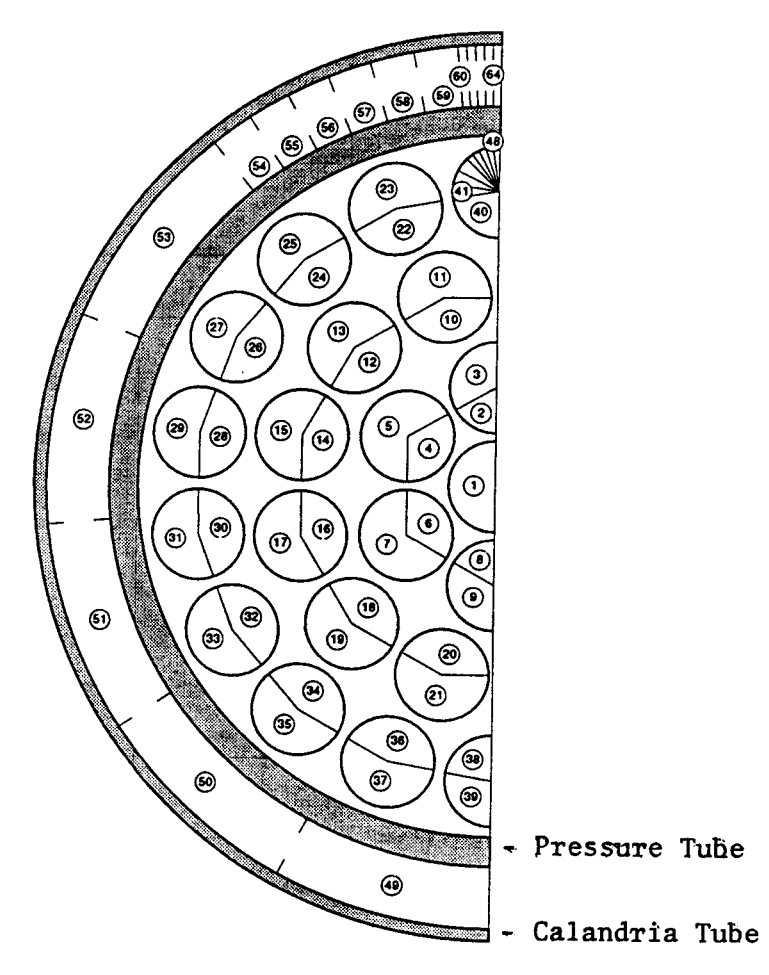


FIGURE 2 Sectoring of Channel in CATHENA Model

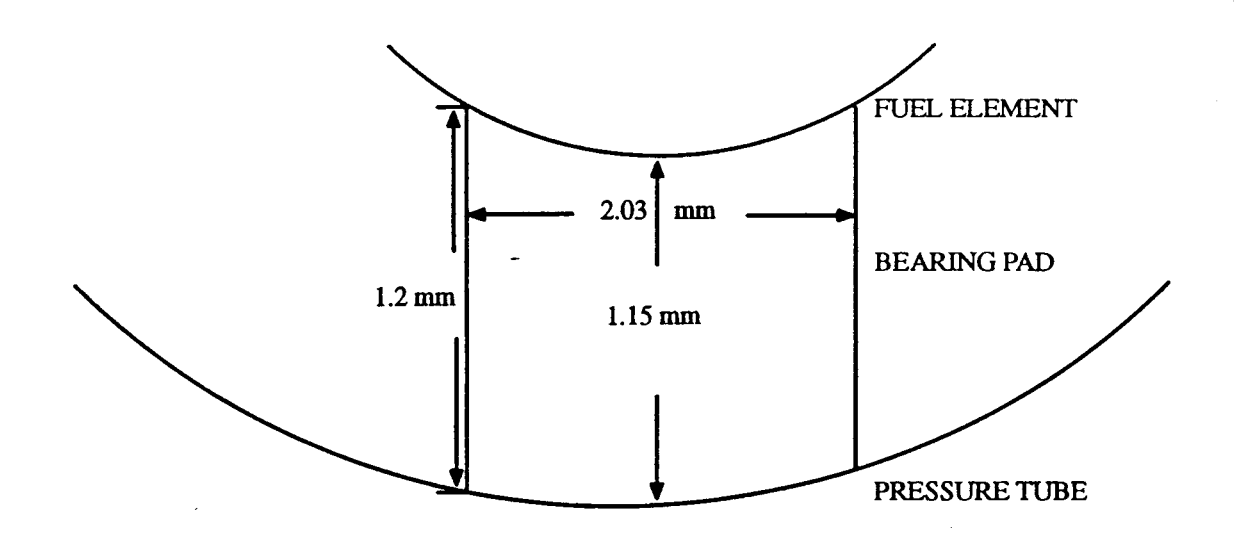


FIGURE 3 STANDARD BEARING PAD DESIGN

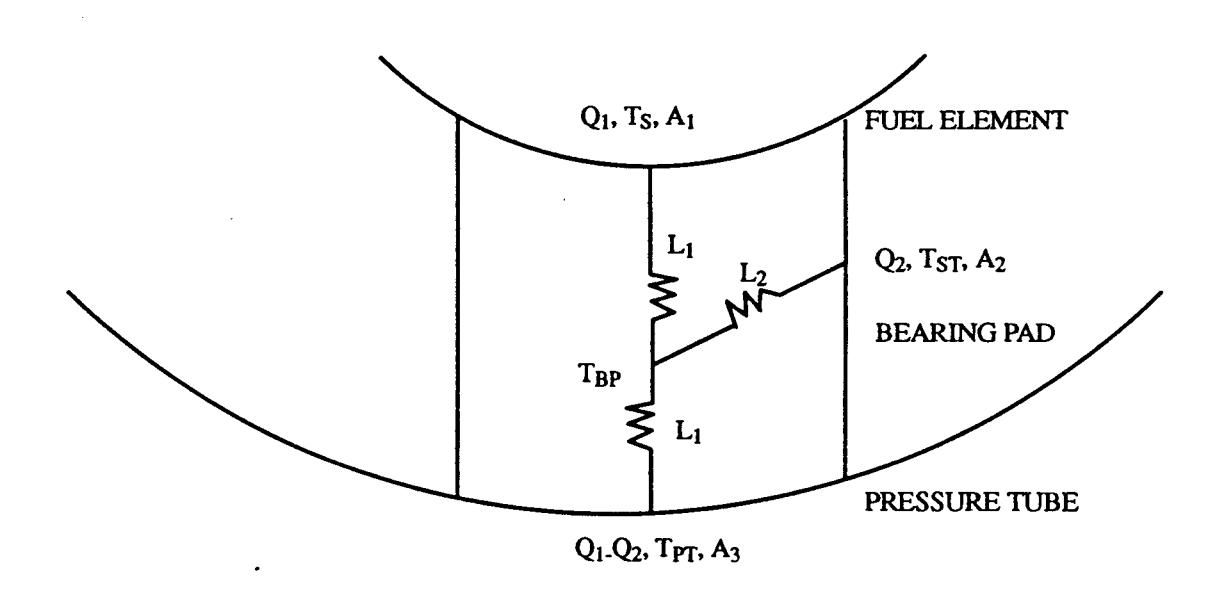


FIGURE 4 ILLUSTRATION OF HEAT TRANSFER MODEL FOR BP/PT CONTACT

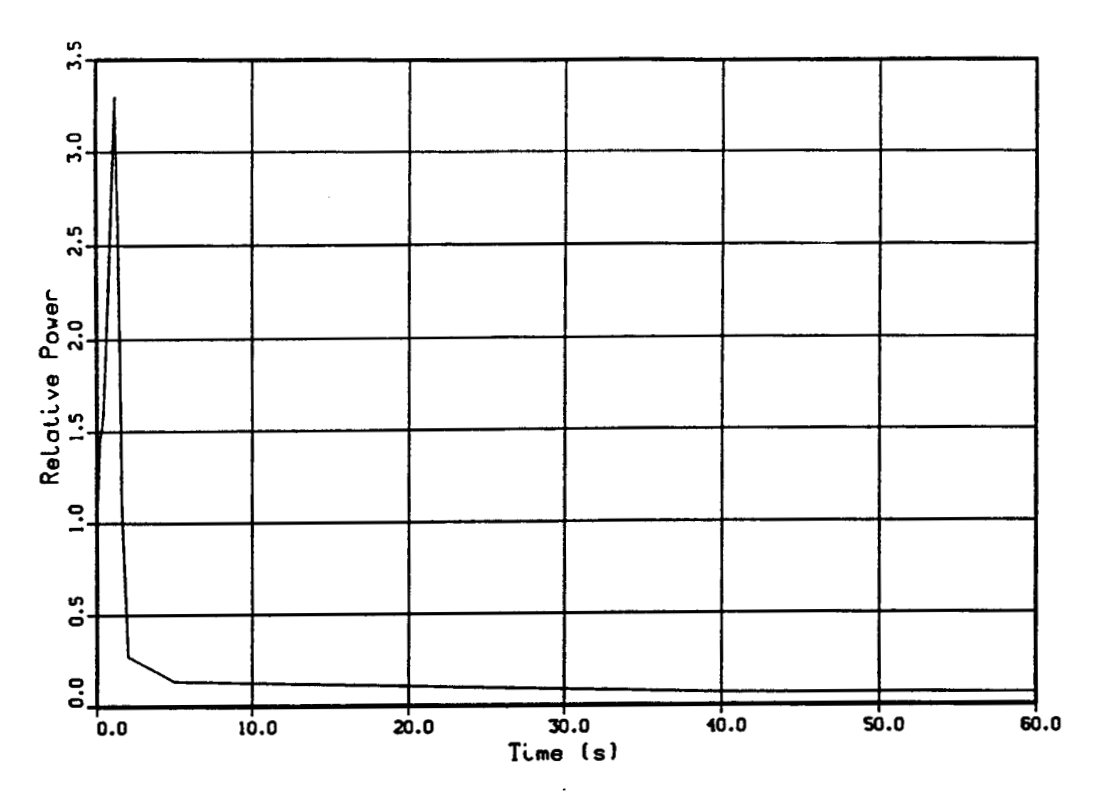


FIGURE 5 Power Pulse Assumed for Test Run

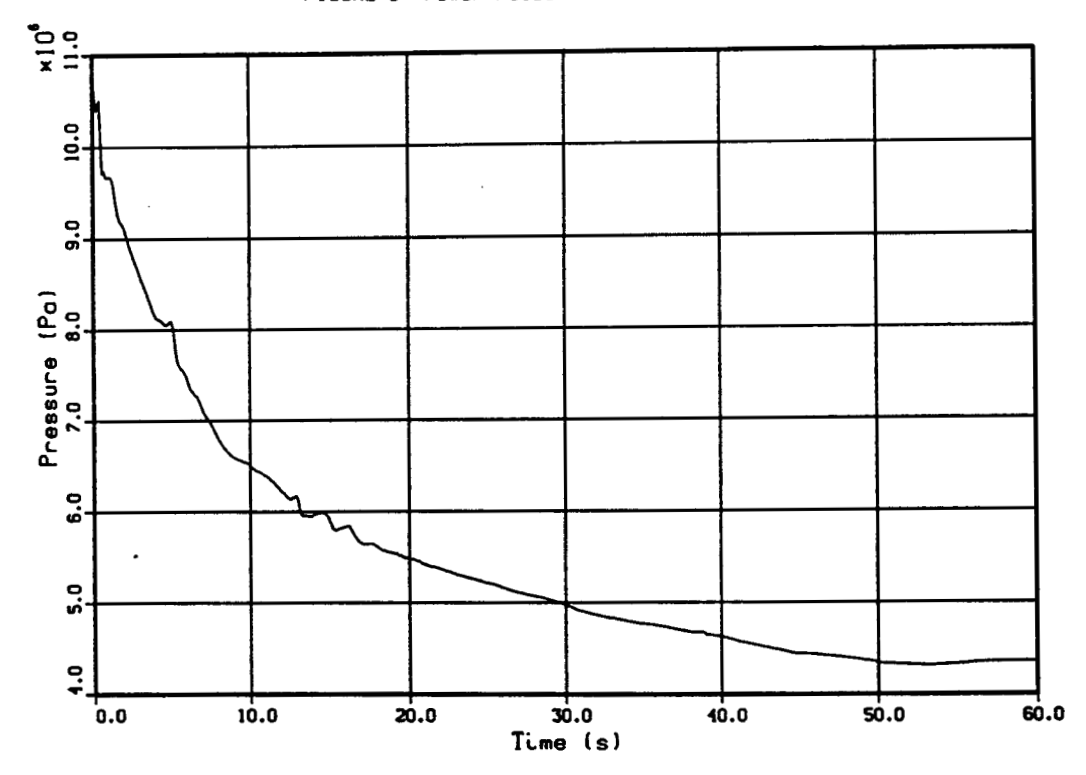


FIGURE 6 Channel Pressure at Bundle 6

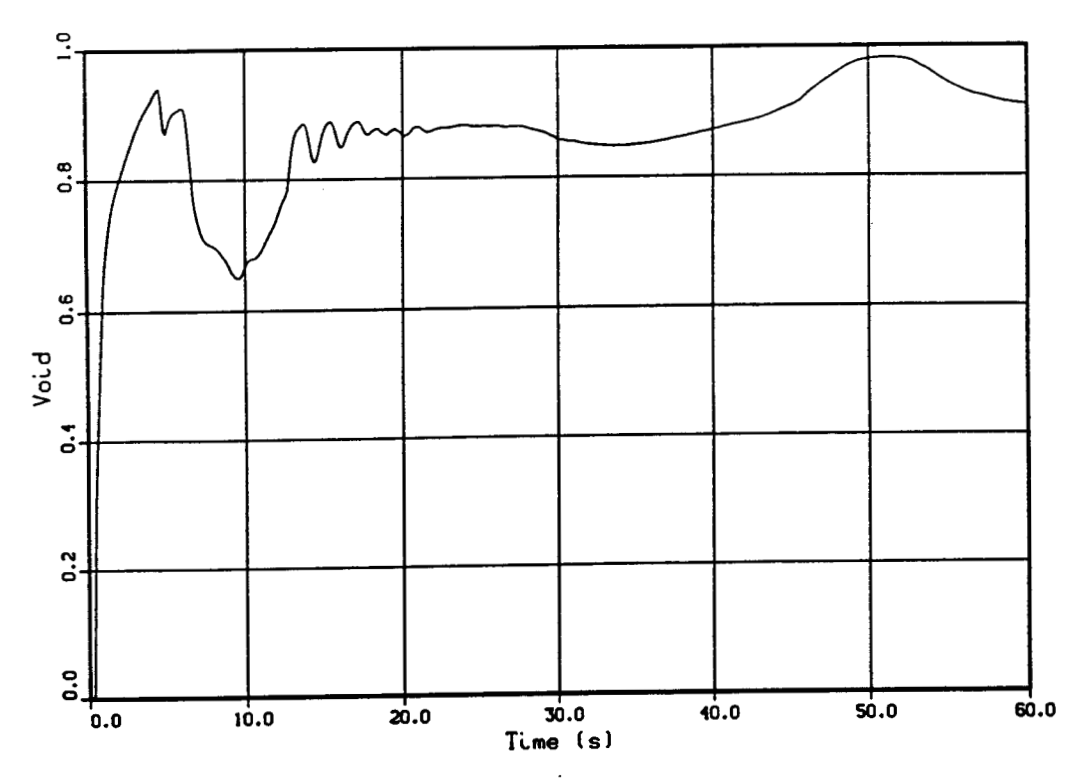


FIGURE 7 Channel Void at Bundle 6

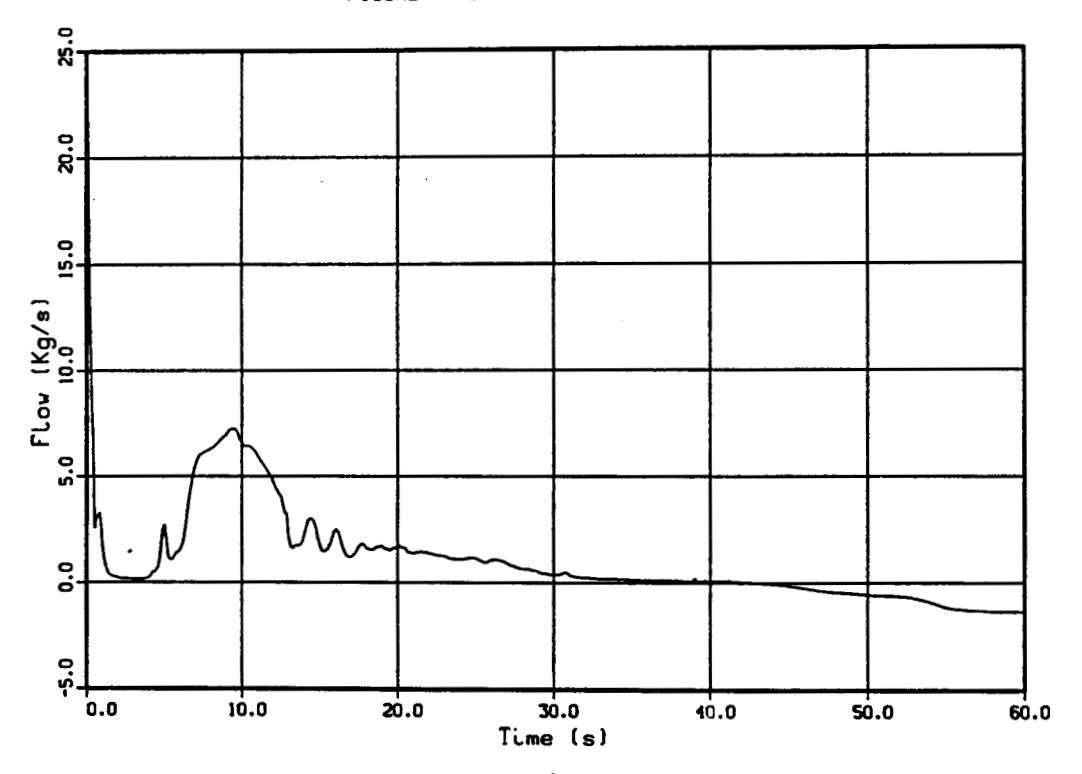


FIGURE 8 Channel Flow at Bundle 6

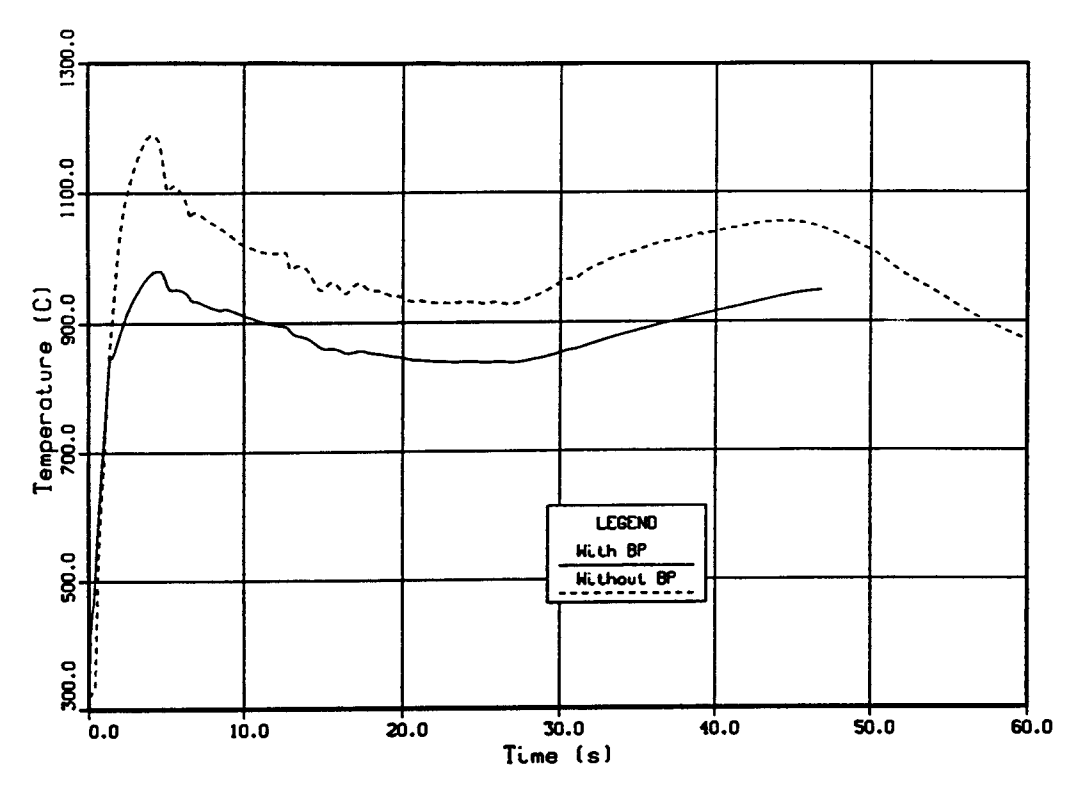


FIGURE 9 Temperatures of Top Element TOP Sector at Bundle 6

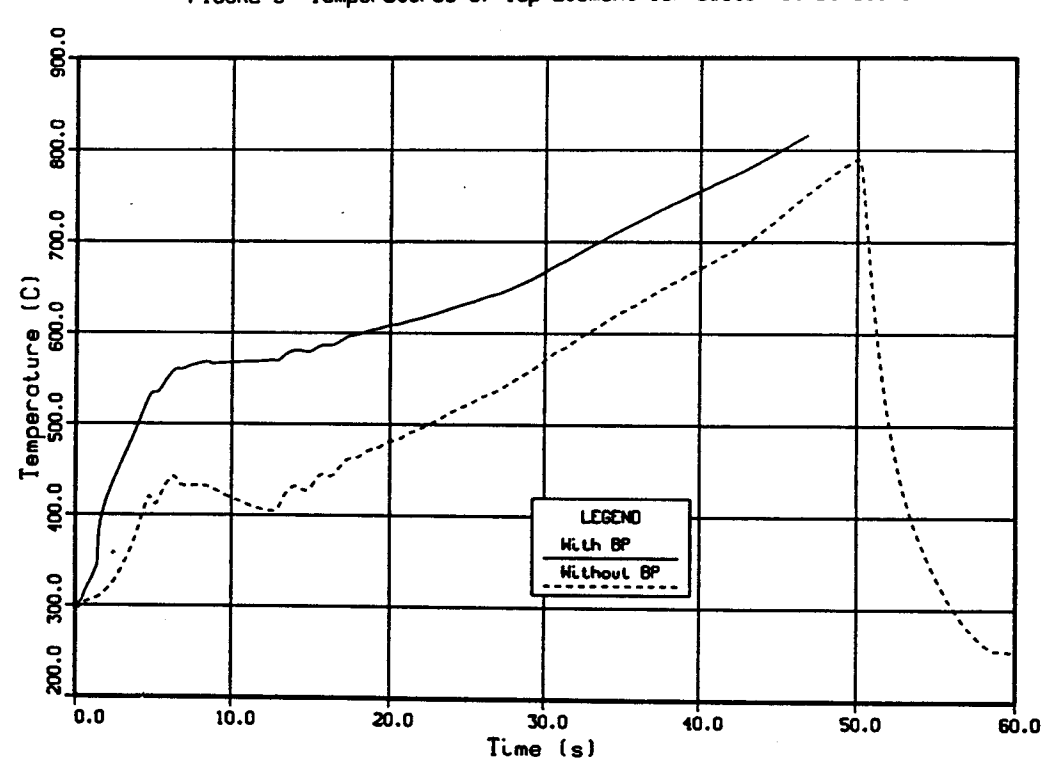


FIGURE 10 Temperatures of Pressure Tube Top Sector at Bundle 6

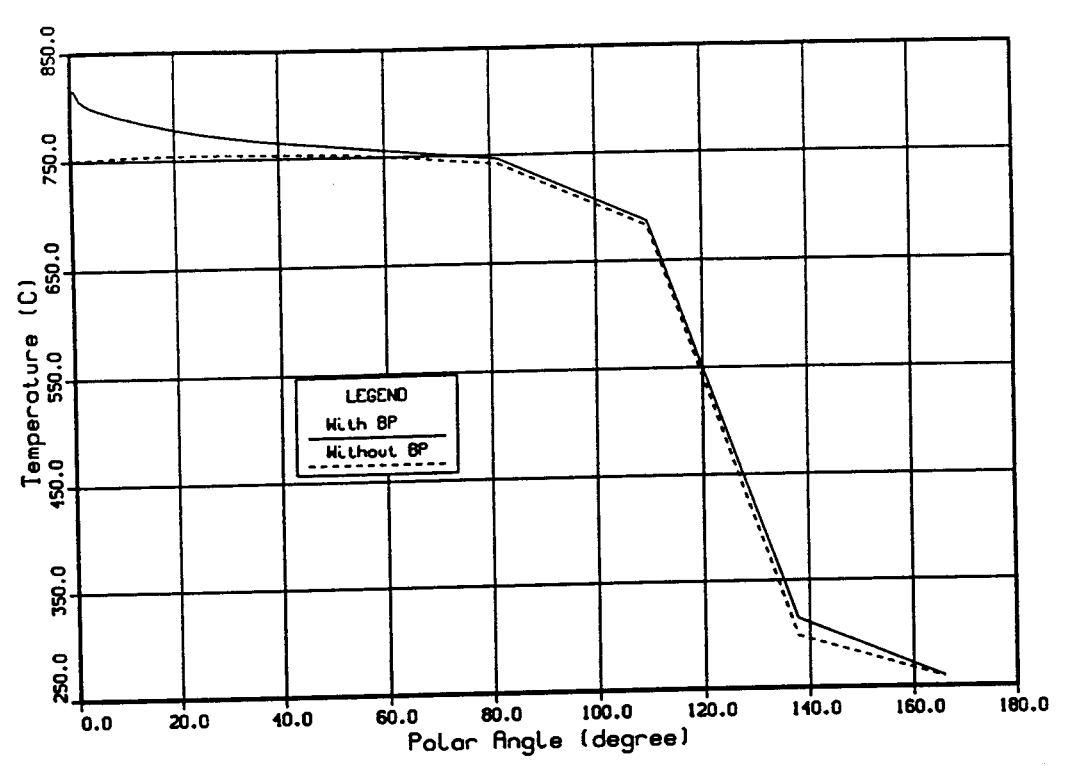


FIGURE 11 Circumferential Pressure Tube Temperature Distribution At 46.8 sec for Bundle 6

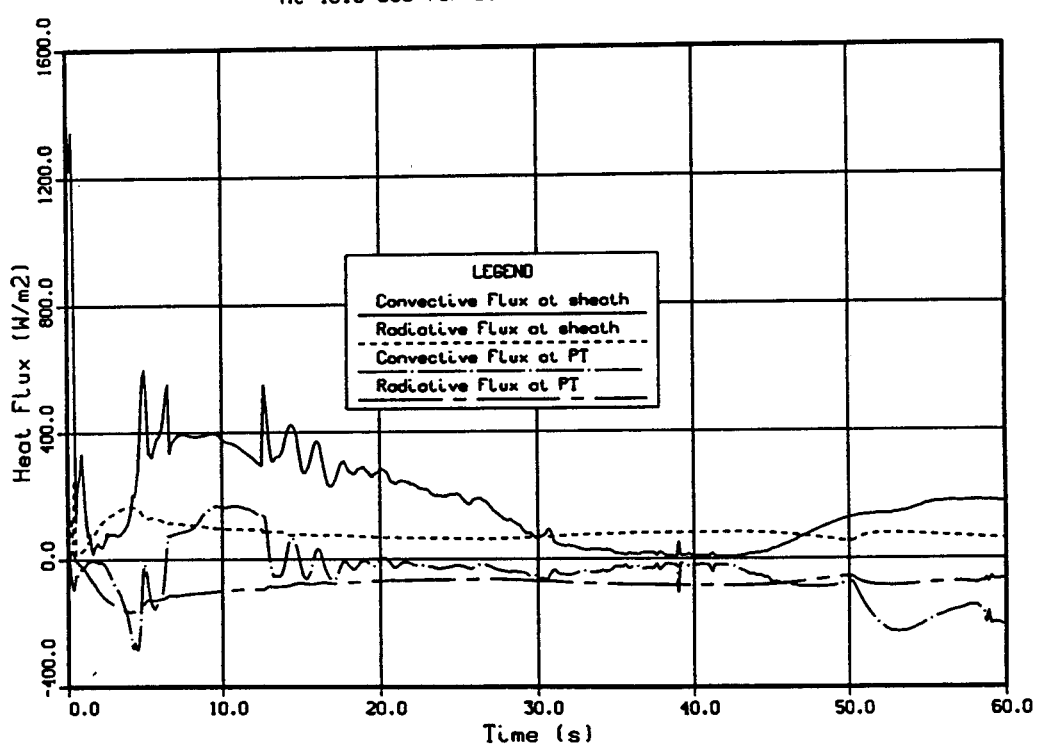


FIGURE 12 Heat Flux Transients at Top Element Sheath Outside and Pressure Tube Inside Surfaces

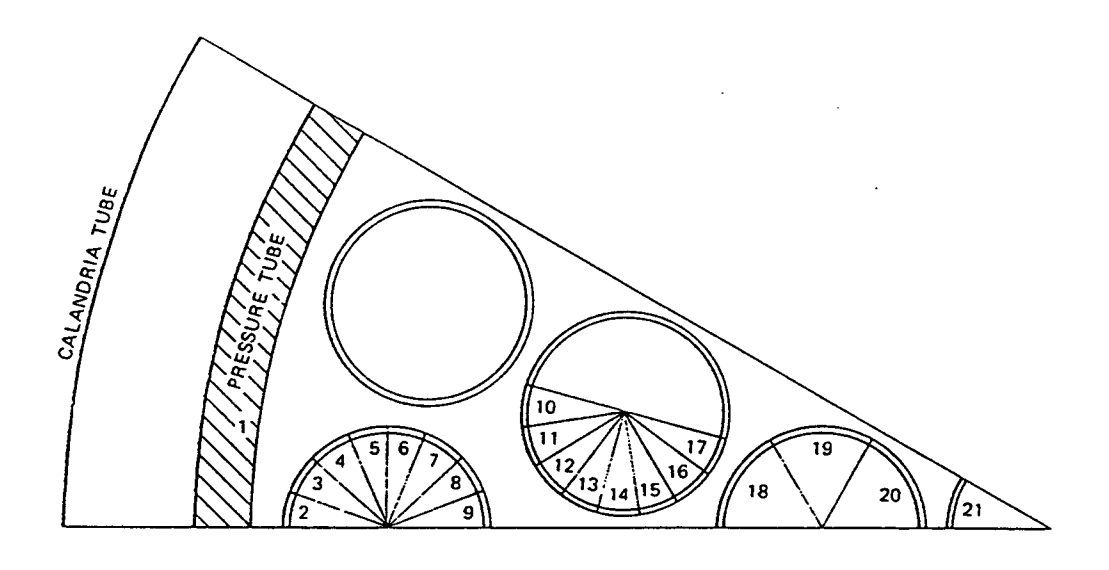


Figure 13 HOTSPOT MODEL OF 37-ELEMENT FUEL BUNDLE SHOWING CIRCUMFERENTIAL NODES

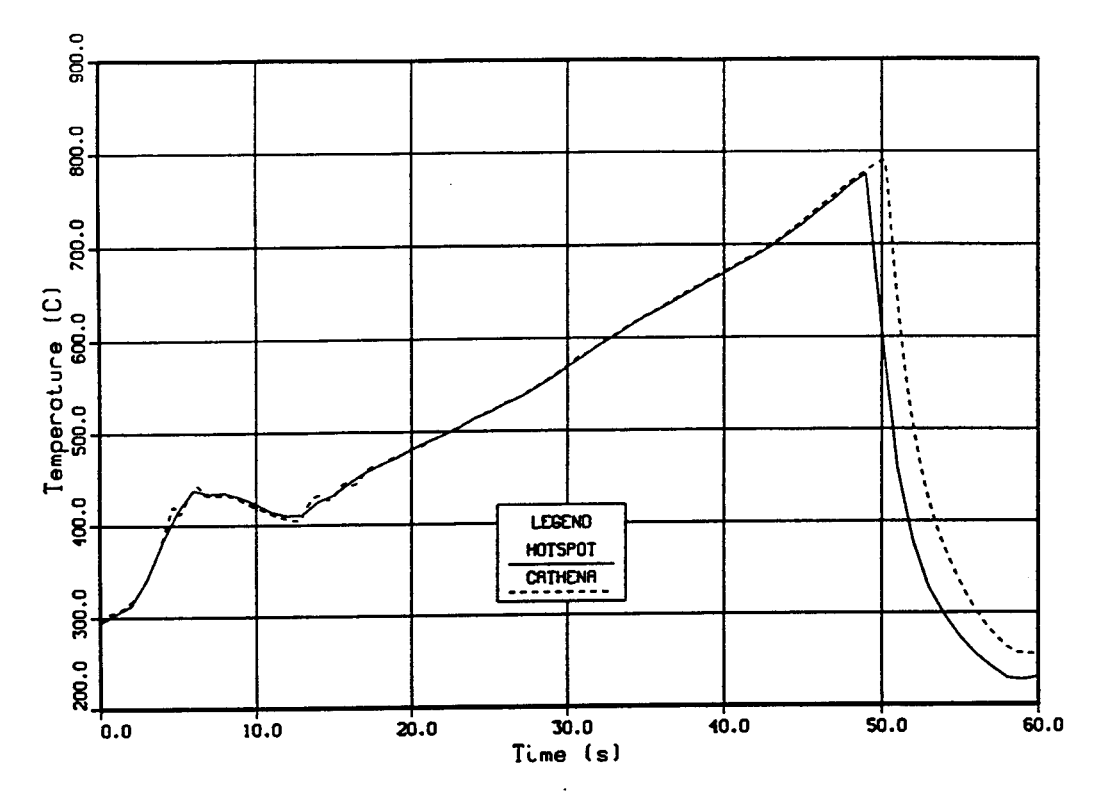


FIGURE 14 Temperature Transients of Pressure Tube Inside Surface (Sector 1 in Figure 13 & Sector 64 in Figure 2)

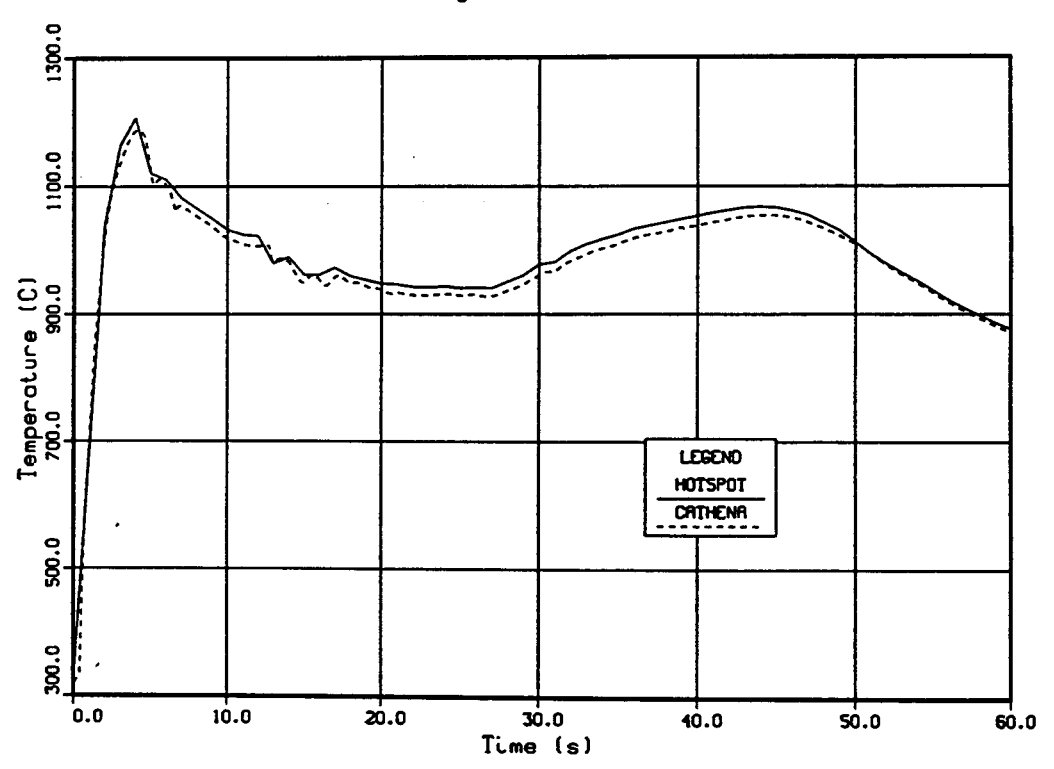


FIGURE 15 Temperature Transients of Top Element Outside Surface (Sector 2 in Figure 13 & Sector 48 in Figure 2)

,				
	×			
	,			